Acta Math. Univ. Comenianae
Vol. (submitted to AMUC), pp. 1–18

COMPUTING MINIMAL SURFACES BY MEAN CURVATURE FLOW WITH AREA-ORIENTED TANGENTIAL REDISTRIBUTION

L. TOMEK, M. REMEŠÍKOVÁ AND K. MIKULA

Abstract. In this paper we use a surface evolution model for construction of minimal surfaces with given boundary curves. The initial surface topologically equivalent to a desired minimal surface is evolved by mean curvature flow. To improve the quality of the mesh we propose an area-oriented tangential redistribution of the grid points. We derive the numerical scheme and present several numerical experiments.

1. Introduction

The goal of this paper is to present a surface evolution technique for computing minimal surfaces employing the mean curvature flow as an evolution model. The mean curvature flow is enriched with suitable tangential velocity in order to redistribute the mesh points along the surface. The work is based on ideas developed in the paper [**21**]. The area-oriented tangential redistribution for surfaces with boundary and its application for computing the minimal surfaces is new and forms the main contribution of the paper.

The mean curvature flow was originally proposed as a model for description of the evolution of the interfaces in multiphase physical models [**27**]. Since minimal surfaces (surfaces with zero mean curvature) are the critical points for the mean curvature flow, one can use the mean curvature flow as a tool for constructing minimal surfaces with given boundary curve(s). Such surfaces are used, e.g., in architecture [**15**]. The problem of finding a minimal surface with given boundary curve(s) is called the Plateau problem, named after the Belgian physicist J.A.F. Plateau [**29**] who made experimental studies of soap films. Algorithms based on the mean curvature flow have also been developed in the field of digital image processing because of the "regularizing effect" due to its parabolic nature [**1, 7, 20**].

Two basic approaches are used for solving manifold evolution problems (including mean curvature flow of surfaces in $\mathbb{R}^3$), the Lagrangian approach that evolves

Received ....
2000 *Mathematics Subject Classification.* Primary 53A10, 53C44, 65D17.
Key words and phrases. minimal surface, mean curvature flow, finite volume, tangential redistribution.
This work was supported by projects APVV-15-0522 and VEGA 1/0608/15.

the manifold directly [**9, 2, 21, 11**] and the Eulerian (level set) approach that, in general, considers the n-dimensional manifold as a level set of a function of $n+1$ variables [**12, 7, 30, 28**]. This work follows the Lagrangian approach.

The numerical methods for solving evolution models are usually based on a finite element method [**9, 10, 2**] or a finite volume method [**19, 15, 21**]. In this work we deal with a finite volume method.

Various techniques for tangential redistribution of points have been developed for curves evolving in two dimensions [**14, 17, 22, 23, 3, 31, 5**], three dimensions [**13, 25**] or on 2D surfaces [**24, 6**]. A lot of work has been done for surfaces evolving in $\mathbb{R}^3$ [**2, 16, 26**]. In this paper we generalize a technique for closed surfaces designed in [**21**] to surfaces with boundary.

The text of the paper is organized in several sections. In section 2 we introduce the mathematical model being the mean curvature flow equipped with an area-oriented tangential redistribution. In the section 3 we state a disctretization of the mathematical model by a finite volume method. In section 4 we demonstrate the performance of the method by constructing several minimal surfaces.

2. Mathematical model

Let $F^0 : X \to Y$ be a smooth immersion of a m-dimensional Riemannian manifold (X, g_X) into n-dimensional Riemannian manifold (Y, g_Y), $m \leq n$. The evolution of $X^0 = F^0(X)$ is a one-parameter family of immersions $F : X \times [0, t_f] \to Y$. Given a fixed point $x \in X$, the map $x \mapsto F(x) = F(x, .)$, is a smooth curve on Y. Let $v^t(x)$ denote the vector tangential to the curve at the point $F^t(x) = F(x,t)$ (see Fig. 1), where the map $F^t : X \to Y$ represents a selected immersion from the whole family of immersions. The map $v : X \times [0, t_f] \to TY$, where TY is the tangent bundle of Y, represents the velocity field of the evolution. Thus, the map F is a solution of the equation

$$\partial_t F = v. \tag{1}$$

The evolution equation (1) is coupled with an initial condition $F(x, 0) = F^0(x)$

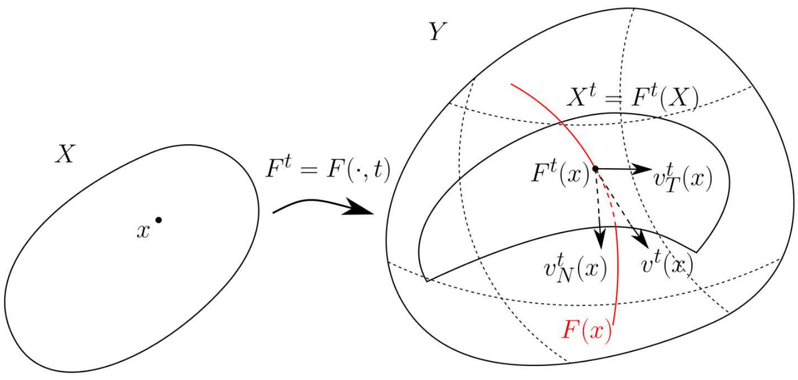

Figure 1. Evolution of a manifold X in a manifold Y.

and, for a manifold X with boundary, with a Dirichlet boundary condition

$$F(x,t) = F^0(x), \qquad x \in \partial X, t \in [0, t_f] \tag{2}$$

meaning the boundary is static. It is convenient to rewrite the velocity v in the form

$$\partial_t F = v_N + v_T, \tag{3}$$

where v_N and v_T are the velocities of the evolution in the normal and tangential direction to the immersed manifold $X^t = F^t(X)$ respectively (Fig. 1). Whereas the normal velocity v_N has an effect on the position and the shape of the immersed manifold X^t, the tangential velocity v_T only moves the points along X^t. In the discrete setting, the tangential velocity v_T can be designed to control the distribution of the mesh vertices, which becomes crucial in numerical computations. An inappropriate placement of the mesh vertices can lead to unacceptable errors or even to a crash of the computation process.

The special type of the evolution model (3) is the mean curvature flow of surfaces with boundary in $\mathbb{R}^3$. That means, X is a two-dimensional manifold with boundary and $Y = \mathbb{R}^3$ with standard Euclidean metric tensor g_Y. The position vector $F(x,t)$ satisfies the evolution model

$$\begin{array}{rrcll} & \partial_t F & = & HN & \\ \text{with} & F(x,0) & = & F^0(x), & x \in X \\ & F(x,t) & = & F^0(x), & x \in \partial X, t \in [0,t_f] \end{array} \tag{4}$$

which means the flow is driven by the normal velocity $v_N = HN$, where $H(x,t)$ and $N(x,t)$ are respectively the mean curvature and the unit normal of the surface $X^t = F^t(X)$ at the point $x \in X$, see Fig. 2. The quantity $h = HN$ is the mean

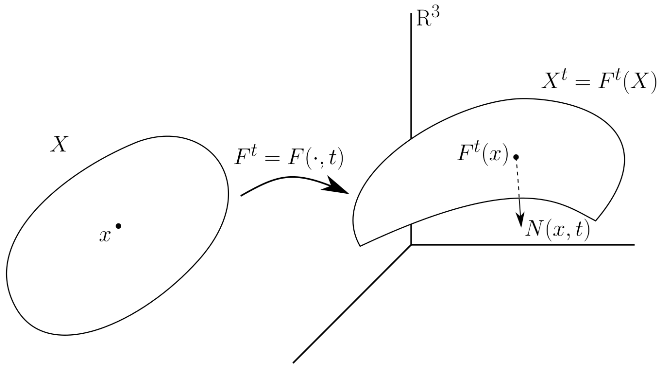

Figure 2. Evolution of a 2-dimensional manifold X in $\mathbb{R}^3$.

curvature vector. Using the formula $h = \triangle_{g_F} F$ (see e.g. [**18**]) we can rewrite the model (4) to the form

$$\begin{array}{rrcll} & \partial_t F & = & \triangle_{g_F} F & \\ \text{with} & F(x,0) & = & F^0(x), & x \in X \\ & F(x,t) & = & F^0(x), & x \in \partial X, t \in [0,t_f]. \end{array} \tag{5}$$

The symbol $\triangle_{g_F}$ denotes the Laplace-Beltrami operator associated with the metric tensor $g_{F^t} = (F^t)^* g_Y$ induced by the immersion F^t, where $(F^t)^*$ denotes the pullback by F^t. To simplify the notation we usually omit the time index t if g_{F^t} is a subscript (as in Laplace-Beltrami operator in (5)). The mean curvature flow may be regarded as a sort of geometric heat equation. On the other hand, the mean curvature flow is not really equivalent to a heat equation, since the Laplace-Beltrami operator evolves with the surface itself.

2.1. The area-oriented tangential redistribution

In our problem only the normal velocity $v_N = HN$ is given. Thus we can enrich the model (5) with a suitable tangential velocity v_T in order to control the area density (defined below) of the discretized evolving manifold.

$$\partial_t F = \triangle_{g_F} F + v_T. \tag{6}$$

In following we state the tangential velocity v_T which strives to achieve uniform area density distribution.

On the manifold X we have the metric g_X and the measure ξ induced by g_X. The metric tensor g_{F^t} induces another measure χ_{F^t} on X. These two measures are related by the following formula

$$d\chi_{F^t} = G^t d\xi, \tag{7}$$

where the map G^t is called the volume density of F^t in general, and in case of evolving surfaces we will call it area density. The evolution of the immersion F^t results in the evolution of the area density. According to [**4**], the map G^t satisfies the following equation

$$\partial_t G = (-g_Y(v_N, h) + \mathrm{div}_{g_F} w_T)G, \tag{8}$$

where w_T is the tangential vector field on X and the operator div_{g_F} represents the divergence on X associated to the induced metric g_F. The vector field v_T on $X^t \subset Y$ is obtained as $v_T = F^t_* w_T$, i.e. the pushforward of w_T along F^t. In case of a manifold with static boundary, the normal component of the tangential velocity w_T vanishes on the boundary, i.e.

$$g_F(w_T, \nu)|_{\partial X} = 0. \tag{9}$$

In [**21**] there are several area-oriented redistributions proposed. We use the asymptotically uniform redistribution which satisfies $\frac{G^t(x)}{A^t} \underset{t\to\infty}{\longrightarrow} C$, where $C \in \mathbb{R}_+$ and A^t denotes the global area of X measured by the measure χ_{F^t}. Using the ideas developed in the paper [**21**] one gets the condition for w_T

$$\mathrm{div}_{g_F} w_T = g_Y(v_N, h) - \langle g_Y(v_N, h)\rangle_\chi + \left(C\frac{A}{G} - 1\right)\omega, \tag{10}$$

where $\langle\,.\,\rangle_\chi$ denotes the mean over X with respect to the measure χ. Now we assume that w_T is a gradient field

$$w_T^t = \nabla_{g_{F^t}} \psi^t, \tag{11}$$

where $\psi^t : X \to R$ is a potential of vector field w_T^t. Under this assumption, we get the following equation for ψ^t

$$\triangle_{g_F}\psi = g_Y(v_N, h) - \langle g_Y(v_N, h)\rangle_X + \left(C\frac{A}{G} - 1\right)\omega. \tag{12}$$

In order to guarantee the uniqueness of ψ^t, the equation (12) is accompanied with an appropriate condition. In this paper we consider manifolds with a static boundary, for which (9) holds. Since velocity w_T has the form (11), we have

$$g_F(\nabla_{g_F}\psi, \nu)|_{\partial X} = 0, \tag{13}$$

which is a natural Neumann boundary condition for ψ^t. Additionally, to ensure the uniqueness of ψ^t, we prescribe the value $\psi^t(P) = 0$ in one selected point $P \in X$.

3. Numerical scheme

In this section we discretize the mathematical model formulated above. The section 3.1 states the cotangent scheme which is a widely used method for computing the numerical solution of the mean curvature flow. In section 3.2 we present a discretization of the tangential velocity.

3.1. Discretization of the mean curvature flow

To discretize the model (6) in the time domain, we apply a semi-implicit approach. The time derivative is approximated by a finite difference and the Laplace-Beltrami operator and the tangential velocity are taken from the previous time step. If τ is the time step, $N = t_f/\tau$ is the number of time steps, $t^n = n\tau$ and $F^n = F(\cdot, t^n)$, we obtain

$$\frac{F^n - F^{n-1}}{\tau} = \triangle_{F^{n-1}}F^n + v_T^{n-1} \tag{14}$$

for $n = 1, \ldots, N$, where the symbol $\triangle_{F^{n-1}}$ denotes the Laplace-Beltrami operator from the previous time step with respect to the metric $g_{F^{n-1}}$ induced by F^{n-1}.

The space discretization is performed using a finite volume method. We approximate the manifold X by a triangular mesh with vertices $x_i, i = 1, \ldots, n_V$. The triangulation of X induces the triangulation of the evolving manifold $X^n = F^n(X)$ with vertices $F_i^n = F^n(x_i), i = 1, \ldots, n_V$. The finite volumes $V_i, i = 1, \ldots, n_V$ are constructed by the barycentric subdivision of the triangulation of X. To obtain the equation for an internal vertex $F_i^n \notin \partial X^n$, one integrates the formula (14) over the finite volume V_i. On the left-hand side we get

$$\int\limits_{V_i} \frac{F^n - F^{n-1}}{\tau} d\chi_{F^{n-1}} \approx A_i^{n-1}\frac{F_i^n - F_i^{n-1}}{\tau} \tag{15}$$

where $A_i^{n-1} = \chi_{F^{n-1}}(V_i)$ denotes the area of the finite volume V_i, and $F^n(x)$ was approximated by its value in the vertex x_i, thus $F^n(x) \approx F_i^n$. For the the

Laplace-Beltrami term on the right-hand side we have (see [**19**] for more details)

$$\int_{V_i} \triangle_{F^{n-1}} F^n \, d\chi_{F^{n-1}} \approx \frac{1}{2} \sum_{p=1}^{m_i} \left(\cot \theta^{n-1}_{i,p-1,1} + \cot \theta^{n-1}_{i,p,2}\right) \left(F^{n-1}_{i,p} - F^{n-1}_{i}\right), \tag{16}$$

with m_i denoting the number of neighbouring vertices of the vertex F_i^n, and where $\theta^{n-1}_{i,0,1} = \theta^{n-1}_{i,m_i,1}$. The angles $\theta^{n-1}_{i,p,1}, \theta^{n-1}_{i,p,2}$ are denoted in Fig. 3.

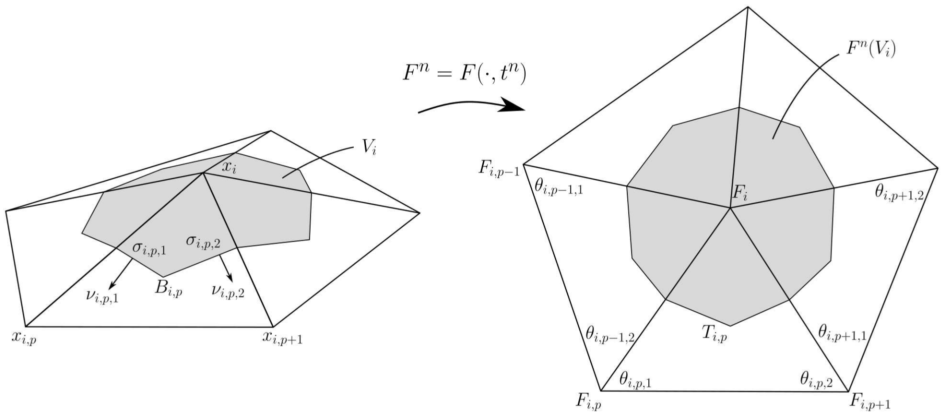

Figure 3. Left, the finite volume V_i around a vertex x_i. Right, the notation in the neighbourhood of the vertex $F_i^n = F^n(x_i)$.

For the tangential velocity term we use the following approximation

$$\int_{V_i} v_T^{n-1} d\chi_{F^{n-1}} \approx A_i^{n-1} \, v_{T,i}^{n-1}$$

where $v_{T,i}^{n-1}$ is the tangential velocity of the vertex F_i^{n-1}. Collecting the terms together we obtain the formula

$$a_i^{n-1} F_i^n + \sum_{p=1}^{m_i} b_{i,p}^{n-1} F_{i,p}^n = F_i^{n-1} + \tau v_{T,i}^{n-1} \tag{17}$$

for $n = 1, \ldots, N$ and each i such that $F_i^n \notin \partial X^n$, and where

$$\begin{aligned} a_i^{n-1} &= 1 + \frac{\tau}{2A_i^{n-1}} \sum_{p=1}^{m_i} \left(\cot \theta^{n-1}_{i,p,1} + \cot \theta^{n-1}_{i,p,2}\right) \\ b_{i,p}^{n-1} &= -\frac{\tau}{2A_i^{n-1}} \left(\cot \theta^{n-1}_{i,p-1,1} + \cot \theta^{n-1}_{i,p,2}\right) \end{aligned}$$

for $p = 1, \ldots, m_i$. The Dirichlet boundary condition (2) is realized trivially as

$$F_i^n = F_i^{n-1}. \tag{18}$$

The equations (17), (18) form a system of n_V linear equations for the unknowns F_i^n, $i = 1, \cdots, n_V$. The initial positions of the vertices F_i^0 are given by the initial condition, i.e. $F_i^0 = F^0(x_i)$.

The mean curvature vector h_i^{n-1} at the point F_i^{n-1} is approximated using cotangent formula (16)

$$h_i^{n-1} = \frac{1}{2A_i^{n-1}} \sum_{p=1}^{m_i} \left(\cot\theta_{i,p-1,1}^{n-1} + \cot\theta_{i,p,2}^{n-1}\right)\left(F_{i,p}^{n-1} - F_i^{n-1}\right). \tag{19}$$

Remark: For simplicity, we fix the boundary points in this paper using (18). In some cases a tangential motion along the boundary may be desirable, since it could improve the mesh quality. On the other hand, it can deform the boundary. There is no deformation in regions where the boundary curve is a line segment, however, the problems arise in regions where the boundary is curved. This is because the approximation of the tangential velocity is not purely tangential and can move the vertices slightly off the curves on which they should be situated. If the boundary has corners, they has to be treated separately because the corners should not move at all. The redistribution along the boundary can be a topic for a further research.

3.2. Discretization of the tangential velocity

In this section we propose a discretization of the equation (12) for surfaces with boundary. To simplify the notation, we omit the time index in some equations. All quantities are taken from the $(n-1)$-th time step. Applying the finite volume technique we integrate (12) over a finite volume V_i. The left-hand side for an internal finite volume V_i ($F_i^n \notin \partial X^n$) reads

$$\int_{V_i} \triangle_{F^{n-1}} \psi^{n-1} d\chi_{F^{n-1}} \approx \frac{1}{2} \sum_{p=1}^{m_i} \left(\cot\theta_{i,p-1,1}^{n-1} + \cot\theta_{i,p,2}^{n-1}\right)\left(\psi_{i,p}^{n-1} - \psi_i^{n-1}\right). \tag{20}$$

For a boundary finite volume V_i (Fig. 4) the integration gives

$$\begin{aligned}
\int\limits_{V_i} \triangle_{F^{n-1}} \psi d\chi &= \int\limits_{\partial V_i} g_{F^{n-1}}(\nabla_{F^{n-1}}\psi, \nu)\, dH_\chi = \int\limits_{\partial V_i - (\partial V_i \cap \partial X)} g_{F^{n-1}}(\nabla_{F^{n-1}}\psi, \nu)\, dH_\chi \\
&\approx \frac{1}{2} \sum_{p=1}^{m_i} \left[\cot\theta_{i,p,2}(\psi_{i,p} - \psi_i) + \cot\theta_{i,p,1}(\psi_{i,p+1} - \psi_i)\right] \\
&= \frac{1}{2} \Bigg[\cot\theta_{i,1,2}(\psi_{i,1} - \psi_i) + \cot\theta_{i,m_i-1,1}(\psi_{i,m_i} - \psi_i) \\
&\qquad + \sum_{p=2}^{m_i-1} \left(\cot\theta_{i,p,2} + \cot\theta_{i,p-1,1}\right)(\psi_{i,p} - \psi_i)\Bigg].
\end{aligned} \tag{21}$$

where the symbol $\nabla_{F^{n-1}}$ denotes the gradient w.r.t. the metric tensor $g_{F^{n-1}}$. Since the boundary of the surface is static, we have $v_N = 0$ for boundary vertices. Thus we can use the following approximation of the first term on the right-hand side in (12)

$$\int_{V_i} g_Y(v_N, h) d\chi_F \approx A_i g_Y(v_{N,i}, h_i) = \begin{cases} A_i H_i^2 & \text{if } F_i^n \notin \partial X^n \\ 0 & \text{if } F_i^n \in \partial X^n \end{cases} \tag{22}$$

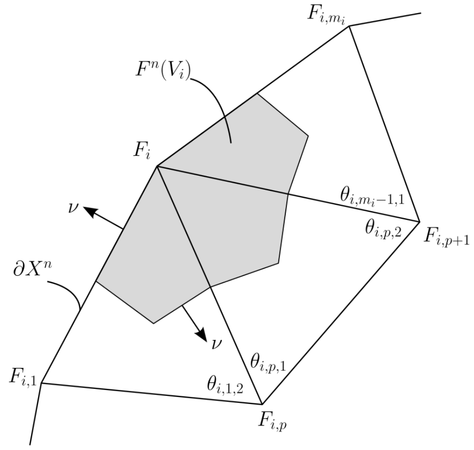

Figure 4. A boundary finite volume.

where $H_i = h_i \cdot N_i$, where N_i denotes the normal to the surface at the point F_i. The approximation of the second term follows

$$\int_{V_i} \langle g_Y(v_N, h)\rangle_{\chi_F} d\chi_F \approx A_i \langle g_Y(v_N, h)\rangle_{\chi_F} \approx \frac{A_i}{A} \sum_{j, F_j \notin \partial X} H_j^2 A_j. \tag{23}$$

where $A = \sum_{i=1}^{n_V} A_i$. Note that the sum in (23) runs over the internal vertices only. For a proper approximation of the last term we introduce an angular size μ_i of a finite volume V_i and a reduced number of mesh vertices n_V^* as follows

$$\mu_i = \frac{\alpha_i}{2\pi}, \qquad n_V^* = \sum_{i=1}^{n_V} \mu_i. \tag{24}$$

For an internal vertex we define $\alpha_i = 2\pi$, resulting in $\mu_i = 1$, and, for a boundary vertex, α_i is the angle between vectors $\overrightarrow{F_i F_{i,1}}$ and $\overrightarrow{F_i F_{i,m_i}}$, see Fig. 4. Now we need to approximate the area density G_i^{n-1}. Since the total surface area A^{n-1} can be computed in two ways

$$\begin{aligned} A^{n-1} &= \int_X d\chi_{F^{n-1}} \approx \sum_{i=1}^{n_V} \chi_{F^{n-1}}(V_i), \\ A^{n-1} &= \int_X G(x, t^{n-1}) d\xi \approx \sum_{i=1}^{n_V} G_i^{n-1} \xi(V_i), \end{aligned}$$

we have $G_i^{n-1} = \frac{\chi_{F^{n-1}}(V_i)}{\xi(V_i)}$. We do not have any conditions imposed on the measure ξ, thus we can set $\xi(X) = \frac{1}{C}$ and

$$\xi(V_i) = \mu_i \frac{\xi(X)}{n_V^*} = \frac{\mu_i}{C n_V^*}.$$

The approximation of the area density follows

$$G_i^{n-1} = \frac{\chi_{F^{n-1}}(V_i)}{\xi(V_i)} = \frac{C n_V^* A_i^{n-1}}{\mu_i}.$$

Finally the approximation of the integral over the last term in (12) is given by

$$\int_{V_i} \left(C\frac{A}{G} - 1 \right) \omega d\chi^{n-1} \approx A_i^{n-1} \left(\frac{A^{n-1}\mu_i}{n_V^* A_i^{n-1}} - 1 \right) \omega. \tag{25}$$

Now we put the approximations (20), (21), (22), (23) and (25) together to obtain the system of equations for ψ_i^n.

Internal vertices

$$\hat{a}_i \psi_i + \sum_{p=1}^{m_i} \hat{b}_{i,p} \psi_{i,p} = H_i^2 - \frac{1}{A} \sum_{j, F_j \notin \partial X} H_j^2 A_j + \left(\frac{A}{n_V^* A_i} - 1 \right) \omega \tag{26}$$

for i such that F_i is an internal vertex, where

$$\begin{aligned} \hat{a}_i &= -\frac{1}{2A_i} \sum_{p=1}^{m_i} (\cot \theta_{i,p,1} + \cot \theta_{i,p,2}) \\ \hat{b}_{i,p} &= \frac{1}{2A_i} (\cot \theta_{i,p-1,1} + \cot \theta_{i,p,2}) \end{aligned}$$

for $p = 1, \dots, m_i$, with $\theta_{i,0,1}^{n-1} = \theta_{i,m_i,1}^{n-1}$.

Boundary vertices

$$\hat{a}_i \psi_i + \sum_{p=1}^{m_i} \hat{b}_{i,p} \psi_{i,p} = -\frac{1}{A} \sum_{j, F_j \notin \partial X} H_j^2 A_j + \left(\frac{A\mu_i}{n_V^* A_i} - 1 \right) \omega \tag{27}$$

for i such that F_i is a boundary vertex, where

$$\begin{aligned} \hat{a}_i &= -\frac{1}{2A_i} \sum_{p=1}^{m_i-1} (\cot \theta_{i,p,1} + \cot \theta_{i,p,2}), \\ \hat{b}_{i,1} &= \frac{1}{2A_i} \cot \theta_{i,1,2}, \\ \hat{b}_{i,p} &= \frac{1}{2A_i} (\cot \theta_{i,p-1,1} + \cot \theta_{i,p,2}) \qquad \text{for } p = 2, \dots, m_i - 1, \\ \hat{b}_{i,m_i} &= \frac{1}{2A_i} \cot \theta_{i,m_i-1,1}. \end{aligned}$$

To make the solution unique, we prescribe the value of $\psi^n, n = 0, \dots, N$ in one selected point, e.g. $\psi_1^n = 0, n = 0, \dots, N$ (in practice we modify the system (26), (27) by replacing corresponding ($i = 1$) equation with $\psi_1 = 0$).

To calculate the tangential velocity $v_{T,i}^{n-1}$ from ψ_i^{n-1} we use the formulas stated in the paper [**21**].

4. Numerical experiments

In all experiments in this section we construct an approximation of a minimal surface with given boundary curve. The initial condition is set as a surface with the same topology as the desired minimal surface. In our implementation the BiCGStab (BiConjugate Gradient Stabilized) method [**32**] was used to solve the systems (17) and (26), (27).

In the first experiment we deal with a roof-like surface. Authors of [**21**] consider the length-oriented redistribution along specific network curves, here we use the area-oriented redistribution. In the initial condition all points are situated in the xy-plane except the points on two of the boundary curves, see Fig. 5, top left. The mesh consist of $n_V = 144$ grid points. Parameters were set to $t_f = 1$, $\tau = 0.01$, $\omega = 50$. We performed the experiments both without any tangential redistribution (Fig. 5) and then with tangential redistribution (Fig. 6). Looking at the figures we observe higher quality mesh of the final minimal surface in case when tangential redistribution is included.

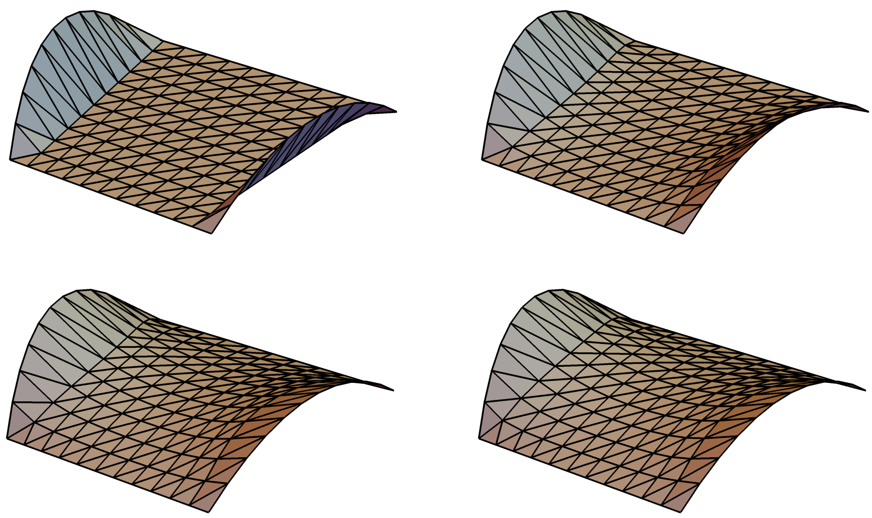

Figure 5. The evolution of a roof-like surface with no tangential redistribution. The selected time steps are $n = 0, 5, 30, 100$.

In the second experiment we construct the approximation of the catenoid which is a minimal surface stretched between two coaxial circles lying in parallel planes. The initial condition is a cylinder (Fig. 7) with boundary circles Γ_1 and Γ_2 defined parametrically as

$$\Gamma_{1,2}(u) = (\cos u, \sin u, \pm\frac{4}{5}\log 2), \qquad u \in (0, 2\pi). \tag{28}$$

We set the parameters to $t_f = 3, \omega = 50$. In this experiment we dealt with two different settings of the time step τ. First, with constant $\tau = 0.04$ for all meshes in

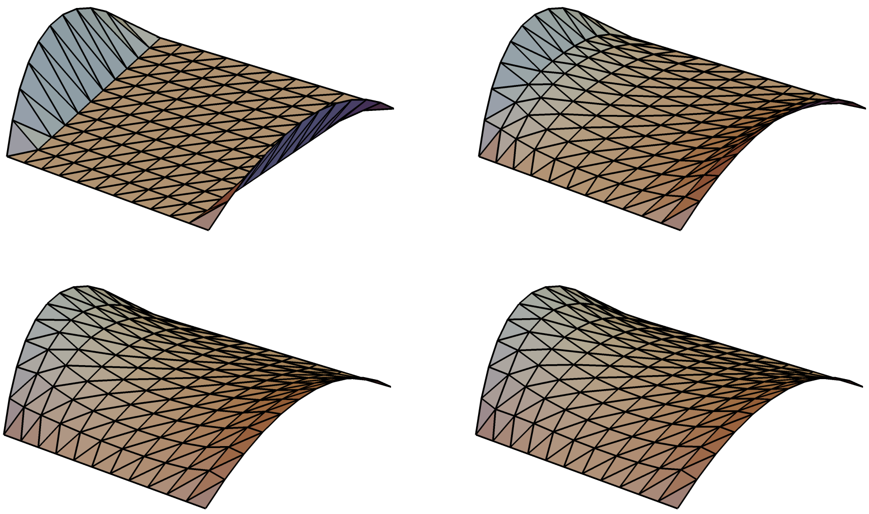

Figure 6. The evolution of a roof-like surface with tangential redistribution. The selected time steps are $n = 0, 5, 30, 100$.

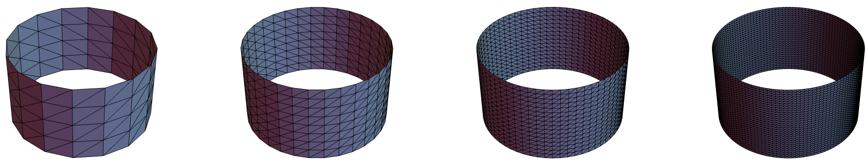

Figure 7. The discretization of the cylinder, from lef to right: $n_V = 80, 288, 1088, 4224$.

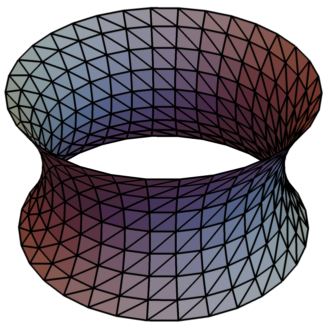

Figure 8. The approximation of the catenoid with $n_V = 288$ vertices in the final time t_f.

Fig. 7, and second, with coupling $\tau \sim h^2$ natural for parabolic problems. The final approximation of the catenoid with $n_V = 288$ is plotted in Fig. 8. The catenoid with the boundary curves (28) is a surface of revolution given by the formula (in cylindrical coordinates r, z)

$$r(z) \quad = \quad \frac{4}{5} \cosh \left(\frac{5}{4} z \right), \tag{29}$$

with $z \in [-\frac{4}{5}\log 2, \frac{4}{5}\log 2]$. The knowledge of the exact solution allows us to calculate the error of the approximation of the catenoid in the final time t_f

$$L_2\text{-error} = \left[\sum_{i=1}^{n_V} \left(\sqrt{(F_{i,x}^N)^2 + (F_{i,y}^N)^2} - r(F_{i,z}^N)\right)^2 \chi_{F^N}(V_i)\right]^{\frac{1}{2}}, \tag{30}$$

where $(F_{i,x}^N, F_{i,y}^N, F_{i,z}^N)$ denote the coordinates of the vertex F_i^N. We also study the experimental order of convergence (EOC) calculated as follows

$$\text{EOC} = \log_2\left(\frac{L_2\text{-error}_h}{L_2\text{-error}_{h/2}}\right), \tag{31}$$

where L_2-error$_h$ is the L_2-error for a mesh with characteristic edge length h. The results are presented in Tab. 1 and Tab. 2. In the tables, "F-iter" and "ψ-iter" are the total numbers of iterations of the BiCGStab method needed to solve the systems (17) and (26), (27) respectively. Comparing Tab. 1 (constant time step

Table 1. The EOC for the case with tangential redistribution, constant time step, $\omega = 50.0$.

n_V	τ	N	L_2-error	F-iter	ψ-iter	EOC
80	0.04	75	1.09e-02	523	1277	
288	0.04	75	2.91e-03	1198	3164	1.91
1088	0.04	75	7.35e-04	2239	6257	1.98
4224	0.04	75	1.81e-04	4975	12873	2.02

Table 2. The EOC for the case with tangential redistribution, coupling $\tau \sim h^2$, $\omega = 50.0$.

n_V	τ	N	L_2-error	F-iter	ψ-iter	EOC
80	0.04	75	1.09e-02	523	1277	
288	0.01	300	2.91e-03	2865	8156	1.91
1088	0.0025	1200	7.36e-04	9880	57498	1.98
4224	0.000625	4800	1.86e-04	31002	266151	1.99

$\tau = 0.04$) and Tab. 2 (coupling $\tau \sim h^2$) we observe that, for this experiment, no refinement of the time step is needed to achieve the same accuracy. The number of iterations per time step is higher for the experiment in Tab. 1, however, the total number of iterations is lower, which results in shorter computation time. Looking at the EOC in Tab. 1 and Tab. 2 we see that the method is second order accurate.

In the third experiment we construct a perturbed catenoid to demonstrate that the method works properly also in the case when the parts of the boundary curve are not convex and even not piecewise planar. The initial condition plotted in Fig. 9 was created by shifting the boundary vertices of the cylinder with $n_V = 288$ vertices shown in Fig. 7. The boundary curves Γ_1, Γ_2 are given by parametric expressions (in cylindrical coordinates (r, ϕ, z))

$$\Gamma_1(u) = (r(u), \phi(u), z(u)) = \left(1 + 0.2\sin^2(3u), u, -\frac{4}{5}\log 2\right), \tag{32}$$

$$\Gamma_2(u) = (r(u), \phi(u), z(u)) = \left(1, u, \frac{4}{5}\log 2 + 0.2\sin^2(2u)\right), \tag{33}$$

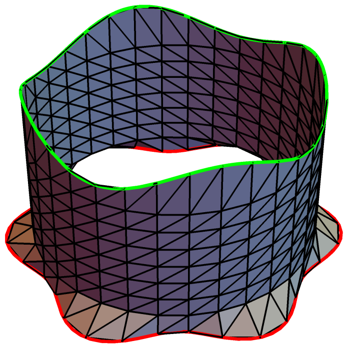

Figure 9. The cylinder with $n_V = 288$ with shifted boundary vertices. Highlighted curves are the boundary curves Γ_1 (bottom, red) and Γ_2 (top, green).

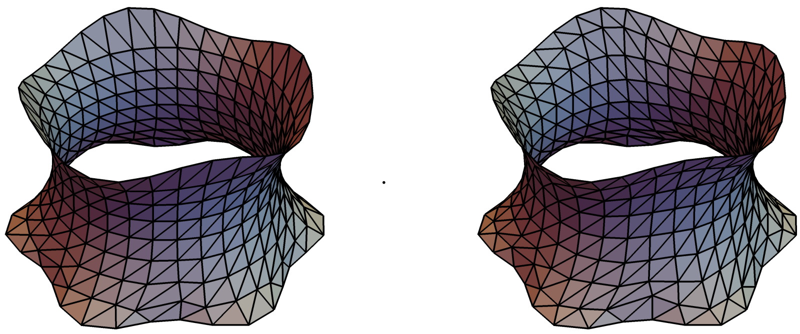

Figure 10. A perturbed catenoid in the last time step $n = 300$. Left, no tangential redistribution. Right, asymptotically uniform tangential redistribution with $\omega = 50$.

where $u \in (0, 2\pi)$, see Fig. 9. We set the final time $t_f = 3$ and time step $\tau = 0.01$. The minimal surfaces for both the case with no tangential redistribution as well as with asymptotically uniform redistribution with $\omega = 50$ are plotted in Fig. 10.

Figure 11. Left, Schwarz P surface. Right, Costa's minimal surface.

In the next experiment we create a minimal surface topologically equivalent to the Schwarz P surface (Fig. 11, left). What we construct is not precisely the Schwarz P surface, since Schwarz P surface is a solution to a different problem, the so-called free boundary problem, where (a part of) the boundary curve is restricted to lie on a given plane instead of being a prescribed curve. The boundary is free to choose its position on the bounding plane. The boundary curves of the Schwarz P surface resemble circles but are not perfect circles. The initial condition in our

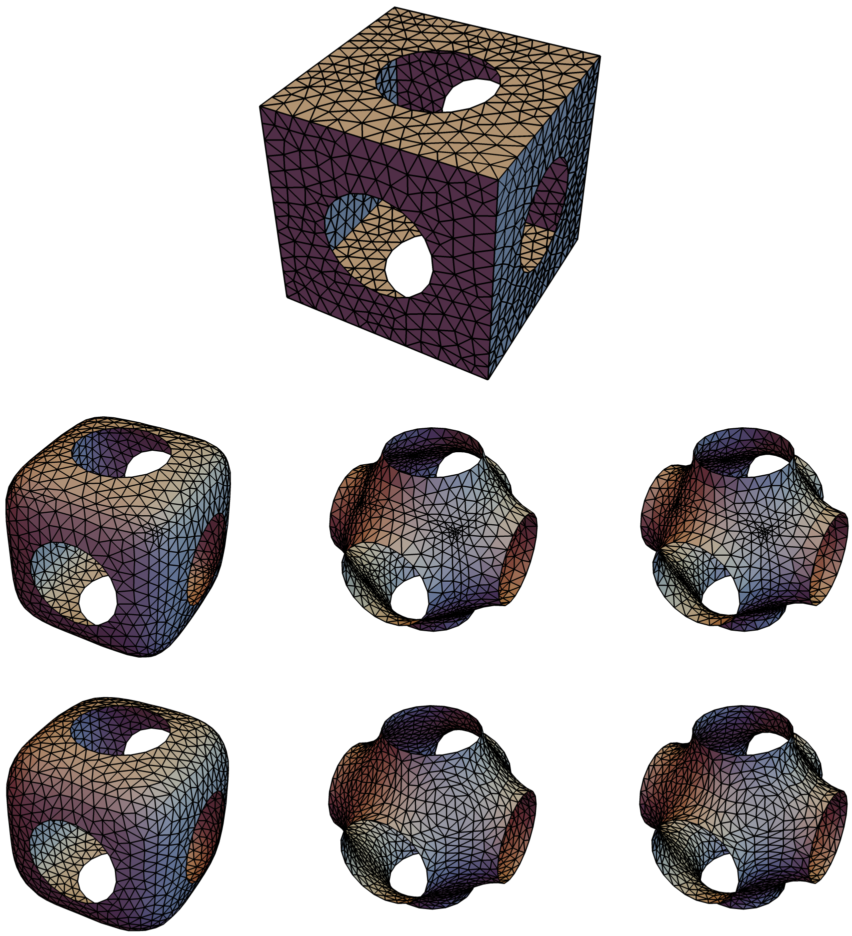

Figure 12. The evolution of the cube with holes into "Schwarz P surface". The first row is the initial condition, the second row corresponds to the evolution with no tangential redistribution, and third row represents the case with tangential redistribution. The selected time steps are $n = 5, 30, 100$.

experiment is a cube with edge length 2 and a circular hole with diameter 1 in the middle of each side. The mesh consists of $n_V = 973$ grid points. The parameters we chose are $t_f = 1, \tau = 0.01, \omega = 50$. The evolution is plotted in Fig. 12. We see that the tangential redistribution helps primarily in the regions of initially high mean curvature (near the corners of the cube).

In the last experiment we construct a minimal surface with topology of the Costa's surface [**8**] (see Fig. 11, right). The initial condition with $n_V = 1438$ grid points is plotted in Fig. 13.

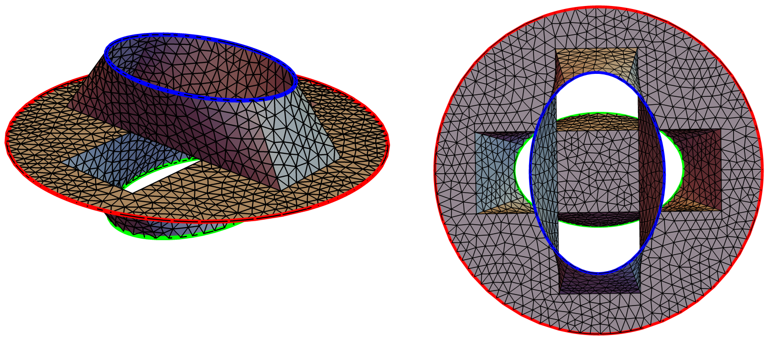

Figure 13. Initial condition for construction of the "Costa's surface". Highlighted curves are boundary curves Γ_1 (middle, red), Γ_2 (bottom, green) and Γ_3 (top, blue).

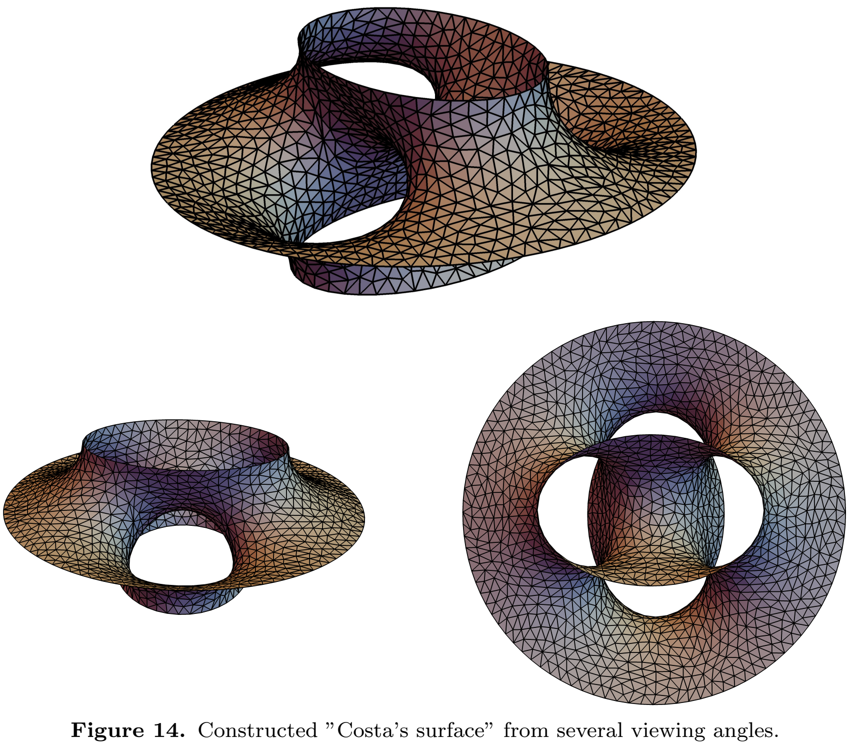

Figure 14. Constructed "Costa's surface" from several viewing angles.

The boundary $\Gamma = \partial X^0$ consists of three curves $\Gamma = \Gamma_1 \cup \Gamma_2 \cup \Gamma_3$, where

$$\begin{aligned}\Gamma_1(u) &= (4\cos u, 4\sin u, 0),\\ \Gamma_2(u) &= (2.25\cos u, 1.5\sin u, -1.5),\\ \Gamma_3(u) &= (1.5\cos u, 2.25\sin u, 1.5),\end{aligned}$$

with $u \in (0, 2\pi)$ for all curves. The parameters were set to $t_f = 1.5, \tau = 0.01, \omega = 5$. In Fig. 14 we see the final approximation of the minimal surface. The Fig. 15

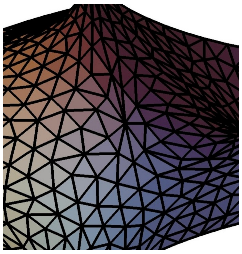

Figure 15. The mesh of the "Costa's surface" in detail with high-valence vertex in the middle.

shows the mesh in detail. In the middle of the figure we see a vertex with $m_i = 10$ with neighbouring triangles with quite acute angles. In order to improve the quality of the mesh near such high-valence vertices it is inevitable to use operations changing the mesh topology, e.g. edge flipping, edge contraction or edge splitting. This can be a topic for a further research.

Conclusion

We presented a surface evolution model with an area-oriented tangential redistribution of points suitable for computing minimal surfaces with given boundary curves. We derived the numerical scheme and performed several numerical experiments to test the performance of the method. Using the model, we constructed approximations of minimal surfaces with given boundary curves.

There are several issues left for a further research. We considered only the area density for designing the tangential velocity, which gives satisfying results in many applications. However, we do not control the shape of mesh triangles which would be necessary in some cases. A tangential redistribution of vertices along the boundary curves could be included to improve the mesh quality. Incorporation of mesh topology changing operations to eliminate high-valency vertices could also improve the the performance of the method. Further, it could be useful to examine other choices of the angular size μ_i. For sake of generality, the method could be extended from triangular meshes to general polygonal meshes.

References

1. Alvarez L., Guichard F., Lions P. L. and Morel J. M., *Axioms and fundamental equations of image processing*, Arch. Ration. Mech. Anal., 123 (1993), pp. 200257.

2. Barrett J. W., Garcke H. and Nurnberg R., *On the parametric finite element approximation of evolving hypersurfaces in* R^3, J. Comput. Phys., 227 (2008), pp. 42814307.
3. Barrett J. W., Garcke H. and Nurnberg R., *The approximation of planar curve evolutions by stable fully implicit finite element schemes that equidistribute*, Numer. Methods Partial Differential Equations, 27 (2011), pp. 130.
4. Bauer M., Harms P., and Michor P. W., *Almost local metrics on shape space of hypersurfaces in n-space*, SIAM J. Imaging Sci., 5(1):244310, 2012.
5. Benninghoff H. and Garcke H., *Efficient image segmentation and restoration using parametric curve evolution with junctions and topology changes, SIAM Journal on Imaging Sciences*, 7(3), (2014), 1451-1483.
6. Benninghoff H. and Garcke H., *Segmentation and Restoration of Images on Surfaces by Parametric Active Contours with Topology Changes*, Journal of Mathematical Imaging and Vision, 55(1), (2016), pp. 105124.
7. Caselles V., Kimmel R. and Sapiro G., *Geodesic active contours*, Int. J. Comput. Vis., 22 (1997), pp. 6179.
8. Costa A., *Examples of a Complete Minimal Immersion in* R^3 *of Genus One and Three Embedded Ends.* Bil. Soc. Bras. Mat. 15, 47-54, 1984.
9. Dziuk G., *Algorithm for evolutionary surfaces Numer. Math. 58 (1991)*, pp. 603-611.
10. Dziuk G. and Elliot C. M., *Finite elements on evolving surfaces*, IMA J. Numer. Anal. 27 (2007), pp. 262-292.
11. Elliott C. M. and Fritz H., *On algorithms with good mesh properties for problems with moving boundaries based on the Harmonic Map Heat Flow and the DeTurck trick*, SMAI J. of Comput. Math., Volume 2 (2016), pp. 141-176.
12. Evans L. C. and Spruck J., *Motion of level sets by mean curvature I*, J. Diff. Geom. 33 (1991), 635681.
13. Hou T. Y., Klapper I. and Si H., *Removing the stiffness of curvature in computing 3-d filaments*, J. Comput. Phys., 143 (1998), pp. 628664.
14. Hou T. Y., Lowengrub J., and Shelley M., *Removing the stiffness from interfacial flows and surface tension*, J. Comput. Phys., 114 (1994), pp. 312338.
15. Húska M., Medl̆a M., Mikula K., Novysedlák P. and Remešíková M., *A new form-finding method based on mean curvature flow of surfaces*, in Proceedings of ALGORITMY 2012, 19th Conference on Scientific Computing, Podbansk, Slovakia, (2012), pp. 120131.
16. Jiao X., Colombi A., Ni X. and Hart J. C., *Anisotropic mesh adaptation for evolving triangulated surfaces*, Engineering with Computers, Vol 26(4): 363-376, 2009
17. Kimura M., *Numerical analysis for moving boundary problems using the boundary tracking method*, Japan J. Indust. Appl. Math., 14 (1997), pp. 373398.
18. Mantegazza C., *Lecture Notes on Mean Curvature Flow*, Addison-Wesley publishing company, Birkhauser Verlag, (2011), 166 s. ISBN 978-3-0348-0144-7
19. Meyer M., Desbrun M., Schroeder P. and Barr A.H., *Discrete differential geometry operators for triangulated 2-manifolds*, Visualization and Mathematics III (H.-C. Hege and K. Polthier, eds.) (2003), pp. 35-57
20. Mikula K., Peyriéras N., Remešíková M. and Smíšek M., *4D numerical schemes for cell image segmentation and tracking*, in Proceedings of Finite Volumes in Complex Applications VI, Problems & Perspectives, Springer-Verlag, Berlin, 2011, pp. 693702.
21. Mikula K., Remešíková M., Sarkoci P. and Ševčovič D., *Manifold evolution with tangential redistribution of points*, SIAM J. Scientific Computing, Vol. 36, No.4 (2014), pp. A1384-A1414
22. Mikula K. and Ševčovič D., *Evolution of plane curves driven by a nonlinear function of curvature and anisotropy*, SIAM J. Appl. Math., 61 (2001), pp. 14731501.
23. Mikula K. and Ševčovič D., *A direct method for solving an anisotropic mean curvature flow of planar curve with an external force*, Math. Methods Appl. Sci., 27 (2004), pp. 15451565.
24. Mikula K. and Ševčovič D., *Evolution of curves on surface driven by the geodesic curvature and external force*, Appl. Anal., 85 (2006), pp. 345362.

25. Mikula K. and Urbán J., *3D curve evolution algorithm with tangential redistribution for a fully automatic finding of an ideal camera path in virtual colonoscopy*, in Proceedings of the Third International Conference on Scale Space Methods and Variational Methods in Computer Vision 2011, Lecture Notes in Comput. Sci. 6667, Springer-Verlag, Berlin, 2011.

26. Morigi S., *Geometric surface evolution with tangential contribution*, J. Comput. Appl. Math., 233 (2010), pp. 12771287.

27. Mullins W.M., *Two-dimensional motion of idealized grain boundaries*, J. Appl. Phys. 27 (1956), 900904.

28. Osher S. and Fedkiw R., *Level Set Methods and Dynamic Implicit Surfaces*, Springer-Verlag, Berlin, (2003).

29. Plateau J. A. F., *Statique expérimentale et téoretique des liquides soumis aux seule forces moléculaires*, volume I, II. Gauthier-Villars, Paris, 1873.

30. Sethian J. A., *Level Set Methods and Fast Marching Methods: Evolving Interfaces in Computational Geometry, Fluid Mechanics, Computer Vision, and Material Science*, Cambridge University Press, New York, (1999).

31. Ševčovič D. and Yazaki S., *Computational and qualitative aspects of motion of plane curves with a curvature adjusted tangential velocity*, Math. Methods Appl. Sci., 35 (2012), pp. 17841798.

32. Van der Vorst H. A., *Bi-CGSTAB: A fast and smoothly converging variant of Bi-CG for the solution of nonsymmetric linear systems*, SIAM J. Sci. Statist. Comput., 13 (1992), pp. 631644.

L. Tomek, Faculty of Civil Engineering, Slovak University of Technology, Radlinského 11, 810 05 Bratislava, Slovak Republic, *e-mail*: `tomek@math.sk`

M. Remešíková, Faculty of Civil Engineering, Slovak University of Technology, Radlinského 11, 810 05 Bratislava, Slovak Republic, *e-mail*: `remesikova@math.sk`

K. Mikula, Faculty of Civil Engineering, Slovak University of Technology, Radlinského 11, 810 05 Bratislava, Slovak Republic, *e-mail*: `mikula@math.sk`